130th ANNIVERSARY OF THE BIRTH OF P.L. KAPITZA

Investigations of new phases of superfluid ^{3}He in nematic aerogel using a vibrating wire

V V Dmitriev, D V Petrova, A A Soldatov, A N Yudin

Contents

Abstract. **The article presents the results of experiments in superfluid ^{3}He, performed using a vibrating wire resonator with a nematic aerogel glued to it, which allowed detecting transitions of ^{3}He to new superfluid phases: to the polar phase, β-phase, and the distorted A- and β-phases. Experiments on observing the A$_1$-phase in a nematic aerogel are also described, where the suppression of the transition temperature was studied, which we associate with the influence of magnetic scattering.**

Keywords: superfluidity of ^{3}He, nematic aerogel, vibrating wire

1. Introduction

Superfluidity of ^{3}He is associated with triplet Cooper pairing with orbital angular momentum and the spin of the pair equal to 1. This type of pairing, in contrast to singlet pairing, allows the existence of several superfluid phases, differing in their structure and properties [1, 2]. Triplet Cooper pairing is also found in some superconductors, including high-temperature ones [3], and, according to theory, in neutron stars [4]. At the same time, superfluid ^{3}He is a convenient object for studying triplet Cooper pairing: its Fermi surface is an ideal sphere, it is

V V Dmitriev [(1, a)], **D V Petrova** [(1, 2, b)], **A A Soldatov** [(1, c)], **A N Yudin** [(1, 2, d)]
[(1)] P.L. Kapitza Institute for Physical Problems,
   Russian Academy of Sciences, ul. Kosygina 2, 119334 Moscow,
   Russian Federation
[(2)] HSE University, ul. Myasnitskaya 20, 101000 Moscow,
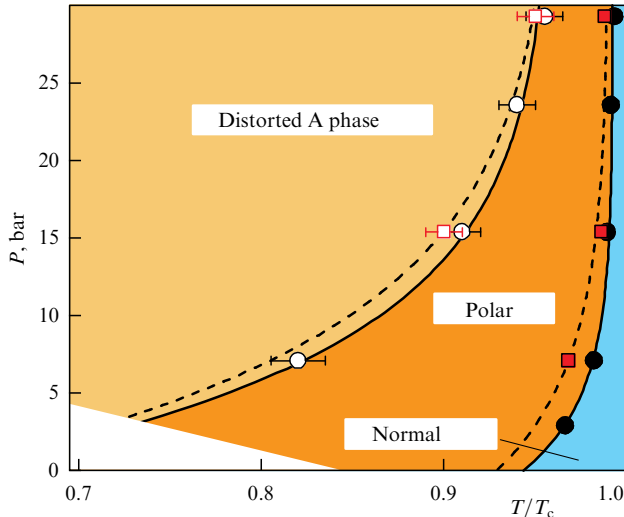   Russian Federation
E-mail: [(a)] dmitriev@kapitza.ras.ru, [(b)] dvpetrova_2@edu.hse.ru,
   [(c)] soldatov_a@kapitza.ras.ru, [(d)] yudin@kapitza.ras.ru

ultrapure at low temperatures, and its coherence length can be varied from 20 to 80 nm by changing the pressure [1].

In the isotropic space in bulk superfluid ^{3}He, the free energy and the superfluid transition temperature are degenerate in the projections of the spin and orbital angular momentum of the pair. Therefore, in practice, only those phases that have the minimal free energy under the given conditions (temperature and pressure) are realized: in the case of pure ^{3}He, they are the so-called A and B phases. The magnetic field changes the energy, making another phase, A$_1$, preferable in a narrow range near the superfluid transition temperature T_c. Therefore, instead of a second-order superfluid transition in a zero field at $T = T_c$, two second-order transitions occur: an 'upper' transition to the A$_1$ phase at $T = T_{A_1} > T_c$ and a 'lower' transition to the A$_2$ phase (also called the A phase in a magnetic field) at $T = T_{A_2} < T_c$. The splitting of T_c (the range of existence of the A$_1$ phase) is proportional to the magnetic field H: $T_{A_1} = T_c + \eta_{A_1} H$ and $T_{A_2} = T_c - \eta_{A_2} H$, where η_{A_1} varies from 0.6 to 4 μK kOe^{-1}, and η_{A_2} varies from 0.6 to 2 μK kOe^{-1} [5–7], depending on the pressure. The temperature range of existence of the A$_1$ phase is $\Delta T = (\eta_{A_1} + \eta_{A_2}) H = \eta_A H$.

The A phase corresponds to the p-pairing model considered by Anderson and Morel. The superfluid gap in this phase is zero at two points on the Fermi sphere. This phase belongs to the class of equal spin pairing (ESP) and consists only of pairs with spin projections 1 and -1 on the preferred direction. The A$_1$ phase appearing in a magnetic field includes only one spin projection $\uparrow\uparrow$, while the A$_2$ phase also contains $\downarrow\downarrow$ states, the portion of which increases as the temperature decreases below T_{A_2}. The B phase is described by the Balian and Werthamer model. Unlike the A phase, the superfluid gap in the B phase is isotropic, so all spin projections are present, including 0.

In ^{3}He, the degeneracy in the orbital angular momentum projections can be removed by introducing global anisotropy into the system, causing the scattering of ^{3}He quasiparticles to

Figure 1. Phase diagram of ^{3}He in nematic aerogel Nafen-72 obtained by NMR method [30]. Dark dots denote T_{ca}; circles denote transition between polar and polar-distorted A phases. White area shows regions without experimental data. Squares and dashed lines show similar data for mullite nematic aerogel, which was used in experiments described below. Aerogel strands were coated with ^{4}He. *x*-axis represents temperature normalized to superfluid transition temperature of bulk ^{3}He, which changes from 0.93 mK to 2.5 mK with increasing pressure.

also become anisotropic. Theory predicts that, if the effective mean free path of ^{3}He quasiparticles along one direction is significantly greater than along others, then new ^{3}He phases — polar, polar-distorted A, and polar-distorted B — may become favorable [8–15]. Aerogels are used to create such anisotropy. Aerogel is a porous material consisting of strands with a diameter of less than or about 10 nm, with an average distance between strands of about 100 nm.

However, experiments with weakly anisotropic silica aerogels have shown that the observed superfluid phases have the same order parameters as the bulk A and B phases of ^{3}He, although the anisotropy affects the phase diagram of superfluidity and the spatial distribution of the order parameter [16–23]. Nevertheless, the polar, polar-distorted A, and polar-distorted B phases have been successfully observed and studied in ^{3}He confined in so-called nematic aerogel [24–26]. Nematic aerogels consist of nearly parallel strands [27], giving rise to strongly anisotropic scattering of ^{3}He quasiparticles inside the aerogel [28, 29]. If the anisotropy is large enough, the superfluid transition of ^{3}He occurs into the polar phase, and, upon further cooling, transitions into the polar-distorted A and polar-distorted B phases are possible. The polar phase (as well as the A phase) belongs to the ESP class and contains Cooper pairs with only ↑↑ and ↓↓ spin projections. However, unlike the A phase, the polar phase is not chiral and has a Dirac nodal line in the energy spectrum of Bogoliubov quasiparticles in the plane perpendicular to the aerogel strands. An example of a phase diagram for ^{3}He in nematic aerogel is shown in Fig. 1.

In addition, it was found that the superfluidity of ^{3}He in nematic aerogels strongly depends on the boundary conditions. The new phases mentioned above are observed if the aerogel strands are pre-coated with a thin (several atomic layers) film of ^{4}He. In the case of pure ^{3}He, the aerogel strands are covered with a solid paramagnetic layer of ^{3}He, which causes a diffuse character of scattering of ^{3}He quasiparticles and includes a magnetic scattering channel.

As a result, the phase diagram for ^{3}He in nematic aerogel changes significantly: near the superfluid transition temperature in aerogel (T_{ca}), instead of the polar phase, the pure A phase is realized, and T_{ca} is noticeably more suppressed [30].

One of the main methods for studying the superfluidity of ^{3}He is nuclear magnetic resonance (NMR), in which phases can be identified, e.g., by measuring the shift of the NMR resonance frequency from the Larmor value. This shift arises due to the dipole interaction of spins in the superfluid condensate and depends on the order parameter, its spatial distribution, and the orientation of the magnetic field relative to the anisotropy axis of the aerogel. However, this method has a significant limitation: the frequency shift is inversely proportional to the magnitude of the magnetic field and becomes small in high fields. This limitation can be circumvented by studying the superfluidity of ^{3}He in aerogel using a vibrating wire (VW) — a resonator immersed in liquid ^{3}He with an aerogel sample attached to it (such experiments with silica aerogels are described in [31–34]). In this case, the appearance of a superfluid fraction of ^{3}He in the aerogel affects the resonance properties of the vibrating wire. This review presents the results of experiments in superfluid ^{3}He, conducted using a vibrating wire with a nematic aerogel glued to it. Experiments on detecting phase transitions in ^{3}He into polar, β, and distorted A and β phases, as well as into the A$_1$ phase (in the case of pure ^{3}He), are described.

2. Vibrating wire

The study of superfluid ^{3}He in aerogels using a vibrating wire is similar to the measurement using a conventional resonator [35, 36]. The mechanical resonance of the wire is excited by the Lorentz force due to an alternating current with amplitude I_0 (from 0.05 to 0.5 mA in our experiments) passed through the wire in a constant magnetic field (Fig. 2). In liquid ^{3}He, the maximum wire velocity at such currents in the temperature range used by us did not exceed 0.1 mm s^{-1}. The motion of the wire creates an alternating voltage, which in our case is amplified by a step-up transformer at room temperature with a coefficient of 1:30 and is measured using a lock-in amplifier. During the experiment, after cooling to the minimum required temperature, measurements are made on a slow warm-up: the dispersion (in phase) and absorption (quadrature) signals are jointly approximated by Lorentz curves to extract the resonance frequency f_a and the absorption line width (resonance width) of the signal Δf_a. In this way, the temperature dependences of the resonance parameters of the vibrating wire are obtained.

In ^{3}He, the resonance frequency of the resonator is inversely proportional to the square root of the oscillating effective mass M. If we use a simple model in which we ignore the effects of ^{3}He flow around the wire and also assume that the mean free path of quasiparticles in bulk ^{3}He is much smaller than the sample size, which is true at the temperatures used, then M has five contributions [33, 37–39]:

(1) the mass of the oscillating part of the wire and the mass of the empty aerogel, the sum of which m_0 determines f_0, i.e., the resonant frequency of the wire with the aerogel in a vacuum;

(2) the mass of the normal component of the liquid inside the aerogel ($m_n = \rho_n^a V$);

(3) the effective mass of the superfluid flow (m_{sf});

(4) the effective mass of the potential back flow of the normal component ($m_{nf} = a\rho_n V$);
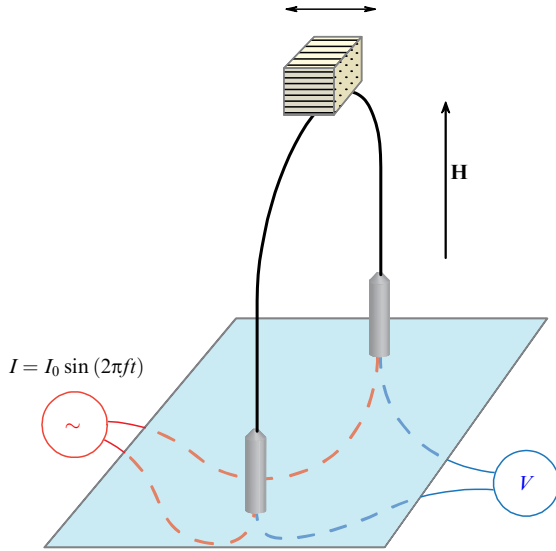
Figure 2. Schematic diagram of measuring the signal of a vibrating wire immersed in ^{3}He liquid in constant external magnetic field **H**. Strands of nematic aerogel glued to wire are oriented along oscillations.

(5) the effective mass m_v carried by the body due to the viscosity of the normal component of liquid ^{3}He ($m_v = b\rho_n V\Delta f_a/f_a$).

Here, V is the volume of ^{3}He in the aerogel, ρ_n^a and ρ_n are the densities of the normal components of ^{3}He in the aerogel and in the bulk ^{3}He, and a and b are the geometric factors (for a sphere, $a = 0.5$ and $b = 1$). The expected resonant frequency is then

$$f_a^2 = f_0^2 \frac{m_0}{m_0 + m_n + m_f + m_{nf} + m_v}\,. \tag{1}$$

Having made a number of assumptions, it can be found that the resonant frequency f_n in normal ^{3}He in the limit $\Delta f_a \to 0$ satisfies the following condition [40]:

$$\frac{1}{f_n^2} - \frac{1}{f_0^2} = \frac{(1+a)V}{m_0 f_0^2}\rho\,, \tag{2}$$

and if $\Delta f_a \ll f_a$, then, for $T > T_{ca}$,

$$f_a = f_n - \frac{1}{2}\,b\,\Delta f_a\,. \tag{3}$$

3. Samples and experimental procedure

In the experiments, two wires and, correspondingly, two samples of nematic aerogel made of mullite ($Al_2O_3SiO_2$) were used, which had a cuboid shape with a size along the strands of ≈ 2.6 mm and characteristic transverse dimensions of ~ 2–3×3 mm. They were cut from a larger piece of the original sample synthesized by Metallurg Engineering Ltd. The cuts were made along the strands so that the final sample had two smooth edges (planes where the strands begin and end) that were not deformed during processing: the irregularities of these edges were about 100 nm. The sample consisted of almost parallel mullite strands with a diameter of $\leqslant 14$ nm (estimated from electron microscope images) and had a total density of ≈ 150 mg cm^{-3}. The density of mullite is 3.1 g cm^{-3}; therefore, the porosity of the sample was 95.2% and the average distance between the strands was 60 nm. In NMR experiments in ^{3}He [25, 41] with a sample cut from the same

piece of aerogel, it was found that, in the presence of a thin ^{4}He coverage of the strands the superfluid transition of ^{3}He in this sample occurs to the polar phase, and that the superfluid transition temperature (T_{ca}) is only slightly suppressed compared to the transition temperature (T_c) of bulk ^{3}He (see Fig. 1). It was also found that, upon further cooling, a second-order transition to a polar-distorted A phase occurs, and that the effective mean free paths of ^{3}He quasiparticles in directions parallel and transverse to the aerogel strands in the limit of zero temperature are ≈ 900 nm and ≈ 235 nm, respectively.

The samples were glued with a small amount of Stycast-1266 epoxy resin to a 240-μm-diameter NbTi wire bent into an arch shape with a total height of 10 mm and a leg spacing of 8 or 4 mm. For these wires, the resonant frequencies in vacuum f_0 were 752 Hz (wire A) and 621 Hz (wire B). The aerogel strands were oriented along the oscillatory motion. The wire with the aerogel was mounted in a cylindrical experimental cell (with an internal diameter of 10 or 6 mm) made of Stycast-1266 epoxy resin and surrounded by a main superconducting solenoid, so that the sample was at the points of the maximum magnetic field (with a uniformity of better than 0.1% over distances of $\leqslant 3$ mm).

The experiments were carried out at pressures from 7.1 to 29.3 bar in magnetic fields up to 19 kOe at temperatures of the order of 2 mK. To obtain such ultra-low temperatures, a nuclear demagnetization cryostat was used, and for pre-cooling, a dilution cryostat was used. To measure the temperature, an additional resonator (a quartz fork) was installed in the experimental cell. The line width of this resonator depends on the viscosity of the surrounding ^{3}He, which allows it to be used as a thermometer after preliminary calibration.

## 4. Results and discussion

4.1 Experiments in normal phase

In our experiments, the viscous penetration depth δ is much smaller than the characteristic dimensions of the aerogel sample, so the observed resonance properties of our vibrating wire at $T > T_c$ are well described by the theoretical model. Figure 3 shows the dependences of the resonance frequency on the resonance width measured at different pressures at $T > T_c$ (unfilled symbols). These dependences are seen to be consistent with Eqn (3). The solid lines in Figure 3 are linear fits to the data, which allow us to determine f_n and b. We find that at all pressures b is close to 1, which is the value expected for a sphere. The obtained values of f_n are also consistent with Eqn (2) (see the inset in Fig. 3): the slope of the line in the inset is 12.7×10^{-6} cm^3 s^2 g^{-1}, while the slope value calculated using Eqn (2) (with $a = 0.5$ and an estimate of $m_0 \approx 5.1$ mg) is 11.6×10^{-6} cm^3 s^2 g^{-1}. Note that the dependence of f_a on Δf_a remains the same for $T_{ca} < T < T_c$ (filled symbols in Fig. 3). Based on our experience of using vibrating wires without aerogel, it can be assumed that this dependence should satisfy Eqn (3) down to $T \sim 0.6T_c$.

4.2 Observation of polar phase

As mentioned above, the superfluidity of ^{3}He in nematic mullite aerogel was previously investigated using NMR methods. In particular, a phase diagram of ^{3}He was obtained under the condition of covering the aerogel surface with ^{4}He (see Fig. 1). At temperatures corresponding to phase transitions, one can expect the appearance of features in the
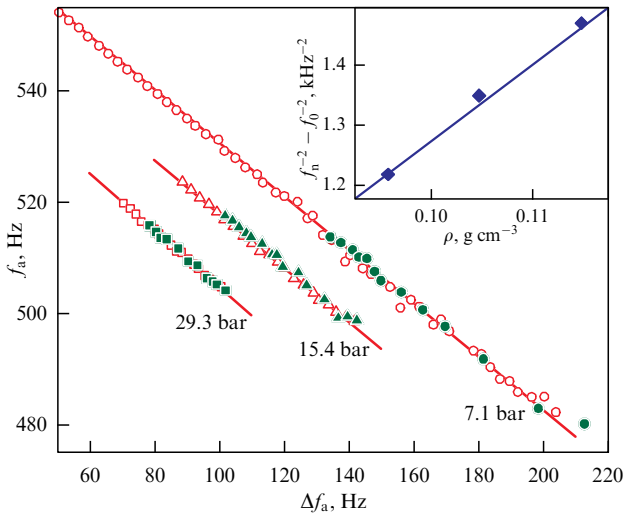
Figure 3. Resonance frequency of a vibrating wire A as a function of resonance width, measured at pressures of 29.3 bar (squares), 15.4 bar (triangles), and 7.1 bar (circles) [40]. Open symbols correspond to measurements in normal ^{3}He ($T > T_c$), filled symbols are obtained at $T_{ca} < T < T_c$. Solid lines are fits to data at $T > T_c$ using Eqn (3) (squares: $b = 1.022$, triangles: $b = 0.973$, circles: $b = 0.962$). $I_0 = 0.25$ mA, $H = 1650$ Oe. Inset: f_n versus ρ determined from linear fits shown in main figure. Solid line is approximation by Eqn (2).
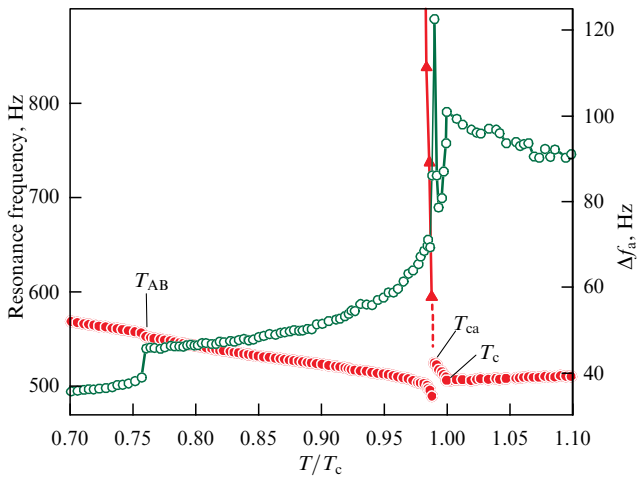
Figure 4. Temperature dependences of width of main resonance in wire A (open circles) and frequencies of main (filled circles) and secondary (triangles) resonances [40]. $P = 29.3$ bar, $I_0 = 0.25$ mA, $H = 1650$ Oe. Arrows point to T_{ca}, T_c and AB transition in bulk ^{3}He at $T = T_{AB}$.

dependences of the resonance parameters of the vibrating wire obtained under the same conditions [40].

Figure 4 shows the temperature dependences of the resonance frequency and width for wire A measured at 29.3 bar. Upon cooling in normal ^{3}He, the resonance width increases, and the frequency decreases due to the increase $\propto 1/T^2$ in the viscosity of the Fermi liquid, which corresponds to an increase in m_v. Then, a rapid decrease in the width (increase in frequency) is observed, indicating a superfluid transition in bulk ^{3}He at $T = T_c$. Upon further cooling, a second resonance (filled triangles in Fig. 4) appears, accompanied by a peak in the width of the main resonance. This additional resonance mode appears just below the superfluid transition temperature of ^{3}He. Therefore, it can be concluded that this resonance is associated with the
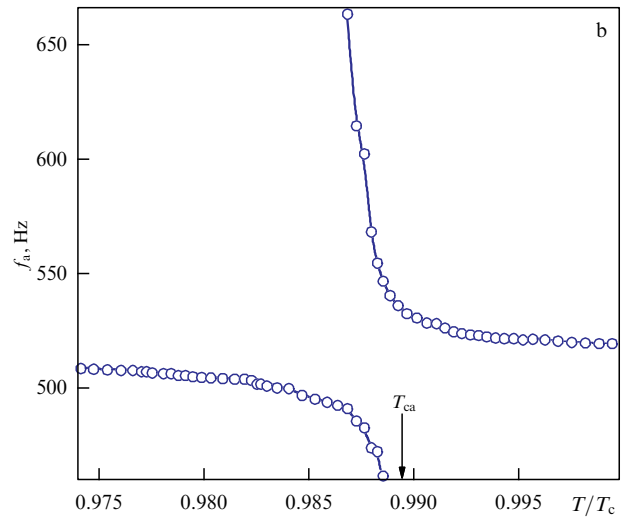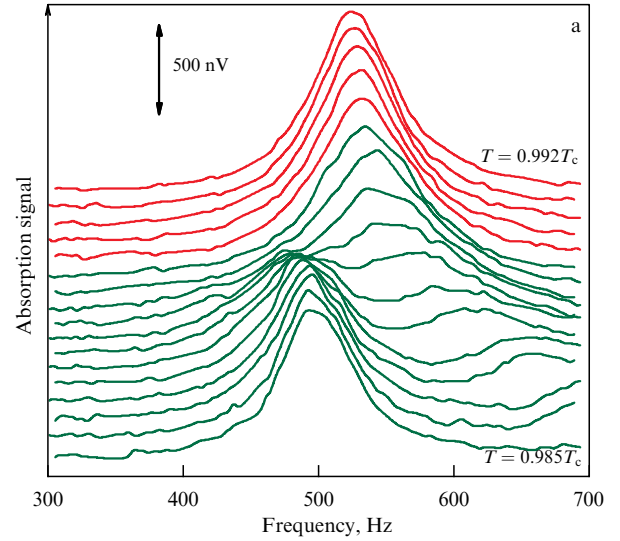
Figure 5. (a) Temperature evolution of absorption signal for a vibrating wire upon slow heating from $T \approx 0.985\,T_c$ to $T \approx 0.992\,T_c$ [40]. For the best view, absorption lines are successively shifted upwards in accordance with increase in temperature. Red and green lines show signals at $T > T_{ca}$ and $T < T_{ca}$, respectively. (b) Two branches of wire resonance as a function of temperature near T_{ca} obtained by fitting lines in panel (a) with sum of two Lorentz peaks. $P = 29.3$ bar, $T_{ca} \approx 0.989\,T_c$, $I_0 = 0.25$ mA, $H = 1650$ Oe.

superfluid transition of ^{3}He to the polar phase in the oscillating sample, which occurs at $T_{ca} \approx 0.989\,T_c$.

Although we were unable to observe a clear resonance peak below 470 Hz, we assume that, upon cooling from $T = T_{ca}$, the frequency of the second mode increases rapidly from 0, and just below T_{ca} becomes close to the main resonance frequency, resulting in interaction (mutual repulsion) between these modes. This is illustrated in Fig. 5a, which shows the evolution of the absorption signal of a vibrating wire when passing very slowly through T_{ca}. Two resonance peaks can be seen just below T_{ca}. The temperature dependence of the resonance frequencies near T_{ca} is shown in Fig. 5b, which demonstrates the repulsion of the two resonance modes. For clarity, below T_{ca} we will always refer to the mode with the lower frequency as the main resonance. Figure 6 shows that, upon cooling, the resonance frequency of the other (second) mode (f_{a2}) increases to about 1600 Hz at $T = 0.75\,T_c$. A similar behavior of this mode was observed at lower pressures.
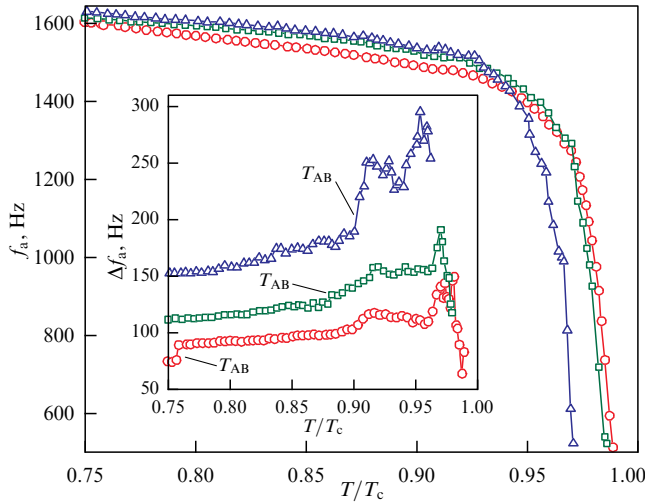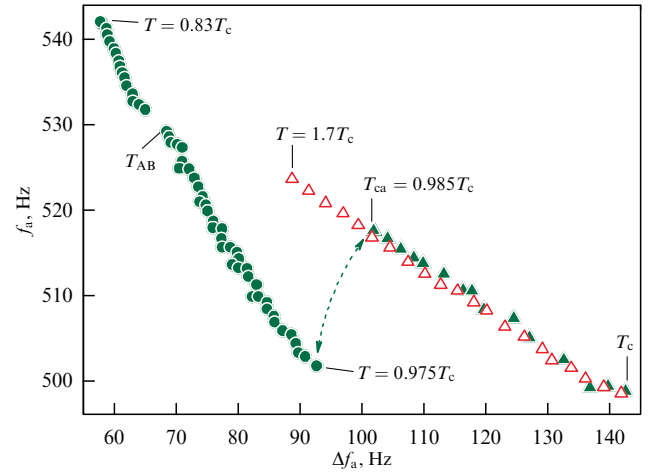
Figure 6. Resonance frequency and resonance width (insert) of second resonance mode in nematic aerogel (wire A) as a function of temperature, measured at $P = 29.3$ bar (circles, $T_{ca} \approx 0.989 T_c$), $P = 15.4$ bar (squares, $T_{ca} \approx 0.985 T_c$), and $P = 7.1$ bar (triangles, $T_{ca} \approx 0.97 T_c$) [40]. Presented superfluid transition temperatures are practically identical to those measured in NMR experiments [41] in a similar sample. $I_0 = 0.25$ mA, $H = 1650$ Oe. T_{AB} is AB transition temperature in bulk ^{3}He.

Figure 7. Frequency of main resonance mode as a function of resonance width, measured at $P = 15.4$ bar in range from $0.83 T_c$ to $1.7 T_c$ (wire A) [40]. Open triangles correspond to measurement in normal ^{3}He, filled triangles correspond to data in the range $T_{ca} < T < T_c$, filled circles correspond to data in the range $0.83 T_c < T < T_{ca}$, $T_{ca} \approx 0.985 T_c$. Data points in the range $0.975 T_c < T < T_{ca}$, where the frequencies and intensities of the resonance modes are close to each other, are not shown.

We assume that the second resonance mode is an analogue of the so-called 'slow' sound mode observed earlier in silica aerogel immersed in superfluid helium [42–44]. The point is that in aerogel the normal component of the liquid is fixed to the matrix, since δ exceeds the characteristic distance between the strands. However, the framework of the aerogel strands is elastic, and the normal component can move together with the strands. Thus, the superfluid component and the combination of the normal liquid and the aerogel matrix can move in opposite directions, which leads to the emergence of an oscillation mode similar to the second sound [42], the resonance frequency of which increases from 0 upon cooling from T_{ca}. In superfluid ^{3}He in silica aerogel, such a resonant mode was successfully observed in low-frequency sound measurements [43, 44]. Here, we are dealing with a highly anisotropic aerogel, which is soft in the direction perpendicular to the strands, but rigid in the direction along the strands. Therefore, in our case, the 'slow' mode should correspond to periodic deformations of the sample in the direction perpendicular to the strands. Note that we are recording the motions of the wire, but we can excite and record the 'slow' resonance mode in the aerogel, even if its frequency is very different from the original resonance of the vibrating wire. This means that, even with significant cooling below T_{ca}, the second resonance mode is significant enough to affect the oscillations of the wire.

Figure 7 illustrates the effect of the second mode on the mail resonance frequency. At $T = 0.975 T_c$, f_a is ≈ 500 Hz, which is 15 Hz less than at $T = T_{ca}$, despite the fact that the second mode frequency continues to increase, although not as quickly as near T_{ca}.

Theoretical studies based on the results of our experiments were undertaken by E V Surovtsev [45–47]; in particular, he managed to approximate the values of the frequencies of the first and second resonant modes near T_{ca} with theoretical dependences.

4.3 Observation of β phase

In the Introduction, it was mentioned that in bulk ^{3}He in strong magnetic fields two second-order transitions occur: to the A_1 phase at $T = T_{A_1} > T_c$ and to the A_2 phase at $T = T_{A_2} < T_c$, instead of a second-order superfluid transition to the A phase (at $T = T_c$).

A similar splitting should also occur in the polar phase in a strong magnetic field [48, 49]. Upon cooling, a superfluid transition to the so-called β phase [1] (or P_1 phase in the notation of E V Surovtsev [48, 49]) is expected instead of a pure polar phase. Upon further cooling, a second-order transition to a distorted β (or P_2) phase should occur. The β phase in ^{3}He has not been observed before, and the use of a vibrating wire has proven useful for an experiment to detect it [50].

The order parameters of the β and distorted β phases are [48]

$$A_{\mu j}^{P_1} = \frac{\Delta_1}{\sqrt{2}} (d_\mu + i e_\mu) m_j \,, \tag{4}$$

$$A_{\mu j}^{P_2} = \frac{\Delta_1}{\sqrt{2}} (d_\mu + i e_\mu) m_j + \frac{\Delta_2}{\sqrt{2}} \exp (i\varphi)(d_\mu - i e_\mu) m_j \,, \tag{5}$$

respectively, where Δ_1 and Δ_2 are the gap parameters, $\exp(i\varphi)$ is the phase factor, **d** and **e** are mutually orthogonal unit vectors in spin space, and **m** is the unit vector in orbital space parallel to the direction of the nematic aerogel strands [8]. From Eqns (4), (5), it follows that the orbital parts of the order parameters of the β and distorted β phases are the same as in the polar phase, but the β phase contains only the ↑↑ state of Cooper pairs, whereas the distorted β phase includes the states ↑↑ (the first term in Eqn (5)) and ↓↓ (the second term in Eqn (5)).

When cooling from the normal phase, the superfluid transition to the β phase should occur at a temperature

$$T_{P_1} = T_{ca} + T_c \eta H \,, \tag{6}$$

where H is the magnetic field, T_{ca} is the superfluid transition temperature of ^{3}He in nematic aerogel at $H = 0$, and $\eta \sim 10^{-3}$ kOe^{-1} [48]. Upon further cooling, a transition to the distorted β phase is expected at temperature

$$T_{P_2} = T_{ca} - T_c \eta H \frac{\beta_{12345}}{-\beta_{15}}, \tag{7}$$

where $\beta_{15} = \beta_1 + \beta_5$, etc., and β_i, $i \in \{1, \ldots, 5\}$ are the coefficients in the Ginzburg–Landau free energy functional [1], or beta parameters. Upon cooling, the distorted β phase continuously transforms into a pure polar phase, i.e., Δ_2 in Eqn (5) becomes equal to Δ_1.

From Eqns (6) and (7), we find that the temperature range of existence of the β phase

$$T_{P_1} - T_{P_2} = T_c \eta H \frac{\beta_{234}}{-\beta_{15}}$$

is proportional to H, and the splitting P$_1$–P$_2$ is characterized by the following equation:

$$\frac{T_{P_1} - T_{ca}}{T_{ca} - T_{P_2}} = \frac{-\beta_{15}}{\beta_{12345}}. \tag{8}$$

Unfortunately, the beta parameters of ^{3}He in nematic aerogel are unknown. Taking the beta parameters of bulk ^{3}He [51] for estimation, we find that the fraction in Eqn (8) is 1.36 at 15.4 bar.

The experiments described in this section were performed with wire B in strong magnetic fields in superfluid ^{3}He in nematic aerogel. The aerogel strands were pre-coated with a sufficient amount of ^{4}He. Most of the experiments were carried out with slow (0.002–0.004 T_c per hour) heating of the cell. Figure 8 shows the results obtained in a magnetic field of 10.25 kOe, where we measured the width Δf_a and frequency f_a of the main resonance of the vibrating wire. In Figure 8, the features (A$_1$, A$_2$, P$_1$, and P$_2$) are marked, which we attribute to transitions at temperatures T_{A_1}, T_{A_2}, T_{P_1}, and T_{P_2}.

Let us consider these features as the temperature decreases. At $T > T_{A_1}$, both bulk ^{3}He and ^{3}He in the aerogel are in the normal state: upon cooling, the width slowly increases and the frequency decreases. The transition to the superfluid state in the A$_1$ phase of bulk ^{3}He occurs at $T = T_{A_1}$. Below T_{A_1} the width decreases, and, at $T = T_{A_2}$, a transition to the A$_2$ phase occurs. The values of T_{A_1} and T_{A_2} obtained by us are close to those measured earlier in Ref. [6].

On further cooling, Δf_a decreases faster, but below $T = T_{P_1}$ it begins to increase, which can only be associated with the transition to the superfluid state of ^{3}He in the aerogel. In this magnetic field, this transition should occur in the β phase. In this case, as in a moderate magnetic field, an additional resonance mode appears, accompanied by a rapid increase in the width of the main resonance in the region just below T_{P_1}.

At a lower temperature (at $T = T_{P_2}$), we observe a 'step' on the Δf_a plot or a 'kink' in the resonance frequency plot, which we attribute to the transition between the β phase and the distorted β phase, which exists at $T < T_{P_2}$.

Note that, upon cooling below $T = T_{P_2}$, the intensity of the second resonance mode begins to grow rapidly, but at $T_{P_2} < T < T_{P_1}$ it is very small. We assume that, in this temperature range (i.e., in the expected β phase), this mode is less excited and, in comparison with the experiments in a
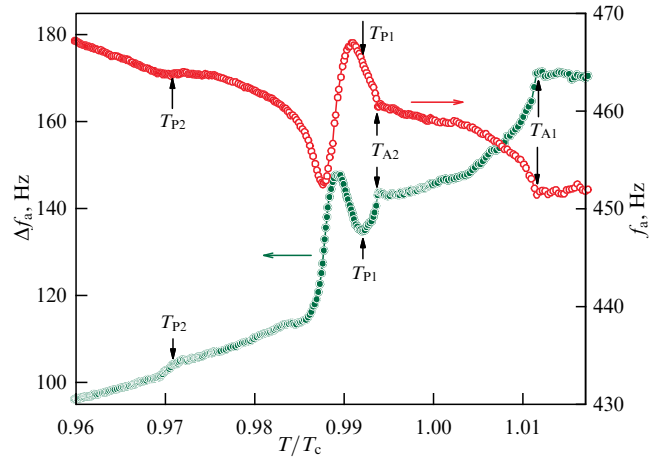
Figure 8. Temperature dependences of Δf_a (filled circles) and frequency (open circles) of main resonance of vibrating wire B, measured in a magnetic field of 10.25 kOe at an excitation current of 0.4 mA [50]. Arrows point to features that we associate with T_{P_2}, T_{P_1}, T_{A_2} and T_{A_1}. T_c is superfluid transition temperature of bulk ^{3}He in a zero magnetic field. $P = 15.4$ bar.
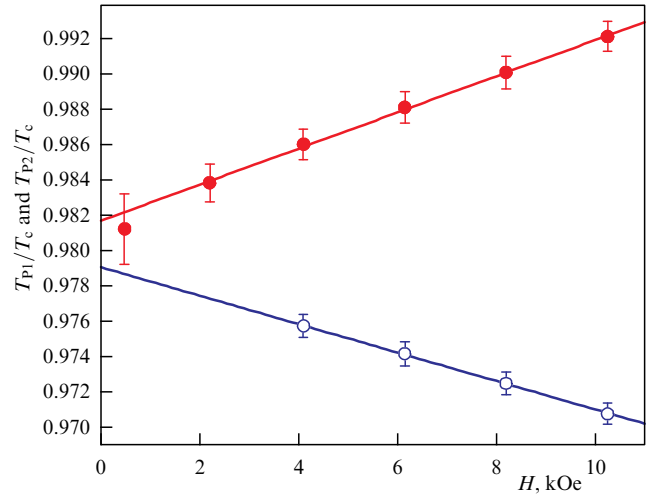
Figure 9. Splitting of superfluid transition temperature of ^{3}He in a nematic aerogel with ^{4}He-coated strands in a magnetic field [50]. Open circles and filled circles indicate transitions between the distorted β phase and the β phase, and between the β phase and the normal phase, respectively. Lines are linear approximations of experimental data.

low magnetic field, we observed no clear repulsion between the main and second resonance modes at $T \approx T_{P_1}$. However, the interaction between them is preserved, and immediately below $T = T_{P_1}$ at the main resonance we observe a peak-like change in the line width, as well as a rapid change in the resonance frequency.

From similar dependences obtained in different magnetic fields, it was determined that, as expected, the temperature range of the existence of the β phase ($T_{P_1} - T_{P_2}$) decreases with decreasing H. Figure 9 shows the dependences of T_{P_1} and T_{P_2} on H, measured at 15.4 bar. The results are well approximated by linear functions, which agrees with the theory. The ratio of the slopes of the approximation lines is

$$\frac{dT_{P_1}/dH}{-dT_{P_2}/dH} = 1.27.$$

According to equation (8), this ratio should be equal to 1.36 if we take into account the β parameters of bulk ^{3}He [51]. Note that the linear approximations do not coincide at $H = 0$. This discrepancy may be due to the finite width ($\sim 0.002 T_c$) of the transition of ^{3}He in aerogel to the superfluid state and may lead to a systematic error of the same order in the determination of T_{P_1}. In any case, it is clear that the temperature range of the existence of the β phase is almost proportional to H, and the splitting value is similar to that observed in the bulk A phase [6, 7].

4.4 Observation of A$_1$ phase

Although the A$_1$ phase in bulk ^{3}He was long ago discovered and has been well studied, the study of its properties in aerogel may offer new perspectives for the analysis of a number of phenomena, such as the influence of spin exchange (the so-called magnetic scattering of quasiparticles) on the superfluidity of ^{3}He, which is manifested in experiments in confined geometry [52].

In the Introduction, it was already said that the A and B phases in aerogel do not differ in the order parameter from the phases realized in bulk ^{3}He. Then, in ^{3}He in aerogel in a strong magnetic field, as well as in bulk ^{3}He, splitting of the superfluid transition should occur and the A$_1$ phase should be observed instead of the A phase. However, in earlier experiments with silica aerogel in fields up to 8 kOe, no splitting was detected [53], and, in high fields (> 70 kOe), a linear dependence on the field was obtained [54, 55]. In theoretical studies, which consider the effect of paramagnetic impurities (which is a thin layer of paramagnetic ^{3}He on strands) on the superfluid transition temperature, it is stated that, in the process of magnetic scattering of ^{3}He quasiparticles by paramagnetic impurities, the spin is not conserved. According to [56, 57], in the presence of spin-exchange interaction, the splitting of the superfluid transition temperature in high magnetic fields is suppressed and in the paramagnetic model is described by the following expression:

$$\Delta T = \left(\eta_0 - C \frac{\tanh(h)}{h} \right) H, \tag{9}$$

where

$$\eta_0 \approx \eta_A \frac{T_{ca}}{T_c}$$

is the splitting parameter in the absence of spin exchange, T_{ca} is the superfluid transition temperature of ^{3}He in aerogel in zero magnetic field, $h = \gamma \hbar H / 2k T_{ca}$, γ is the gyromagnetic ratio, k is the Boltzmann constant, and the spin exchange parameter $C \sim 1$ μK kOe^{-1} depends on the superfluid coherence length, on the mean free path of ^{3}He quasiparticles in aerogel, and on scattering by impurities. The 'upper' transition temperature (T_{ca1}) is determined as follows:

$$T_{ca1} = T_{ca} + \left(\eta_{A_1} \frac{T_{ca}}{T_c} - C_1 \frac{\tanh(h)}{h} \right) H, \tag{10}$$

where, in the weak coupling limit, $C_1 = C/2$.

As mentioned above, in nematic aerogel, in the absence of a ^{4}He strand coating near the superfluid transition temperature (T_{ca}), a pure A phase is realized instead of a polar phase, which means that, just as in isotropic aerogel, the A$_1$ phase should be observed when a magnetic field is introduced, and
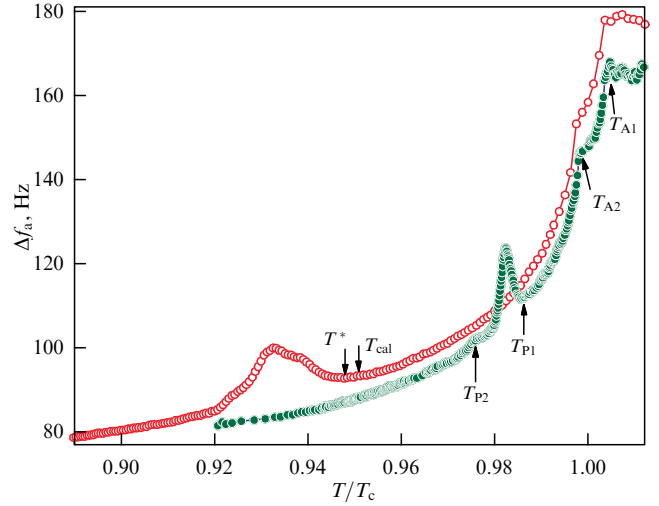

Figure 10. Dependences of width Δf_a of main resonance of a vibrating wire B, measured in the presence of a ^{4}He coating (filled circles, $H = 4.1$ kOe) and in pure ^{3}He (open circles, $H = 4.4$ kOe) [58]. Arrows indicate features that we associate with different superfluid transitions at temperatures T_{P_2}, T_{P_1}, T_{A_2}, T_{A_1}, and T_{ca1} (see text for details). x-axis represents temperature normalized to superfluid transition temperature in bulk ^{3}He $T_c = 2.083$ mK. $P = 15.4$ bar.

the temperature range within which the A$_1$ phase is realized should be suppressed due to spin exchange, as predicted by theoretical studies.

We performed measurements using a vibrating wire similar to those described in the previous section, but without coating the surface with ^{4}He [58]. In Figure 10, the open circles show the obtained temperature dependence of the width Δf_a of the vibrating wire main resonance in pure ^{3}He in a magnetic field of 4.4 kOe. For comparison, the filled circles show a similar dependence obtained in the experiments described above in the presence of a ^{4}He layer at the same pressure and in nearly the same magnetic field (4.1 kOe).

In pure ^{3}He, we observe transitions to the bulk A$_1$ and A$_2$ phases at almost the same temperatures T_{A_1} and T_{A_2} as in the presence of a coating, but the transition to the superfluid state of ^{3}He inside the aerogel occurs at a much lower temperature than the transition temperature T_{P_1}, since the peak change in Δf_a occurs at much lower temperatures. At $T = T_{ca1}$, the wire resonance characteristics upon cooling should begin to deviate from those observed when ^{3}He inside the aerogel remains in the normal phase. Unfortunately, in pure ^{3}He, the local minimum in the temperature dependence of Δf_a (labeled as T^* in Fig. 10) is not sharp enough, and the deviation from the dependence expected when ^{3}He inside the aerogel remains in the normal state begins at a temperature slightly above T^*. Therefore, to determine T_{ca1} in pure ^{3}He, we use the fact that, if ^{3}He inside the aerogel remains in the normal phase, the wire resonance frequency should depend linearly on Δf_a in the temperature range used (see Eqn (3)). Accordingly, we define T_{ca1} as the temperature at which a deviation from such a linear dependence appears upon cooling. This is illustrated in Fig. 11, where the onset of the deviation corresponds to Δf_a equal to 114.1 ± 1.0 Hz. The measured temperature dependence of Δf_a then allows us to find T_{ca1}.

The temperature dependences of the resonance width in magnetic fields from 2.2 to 19.4 kOe were obtained using the method described above. The values of T_{ca1} determined from them increased with increasing H, but we were unable to
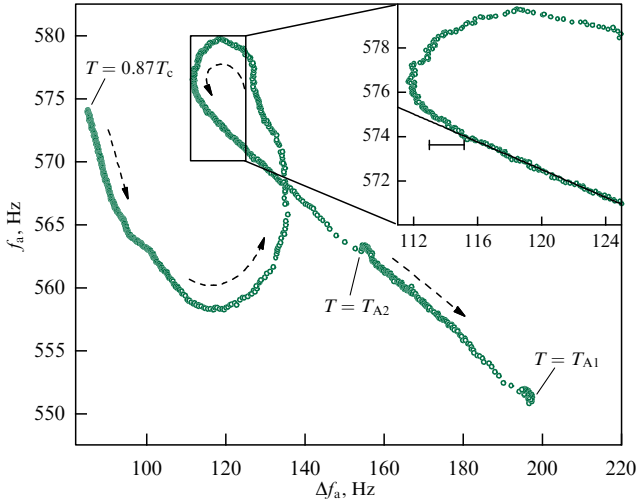
Figure 11. Frequency of main resonance of a vibrating wire as a function of resonance width Δf_a, measured upon heating in a magnetic field of 19.4 kOe [58]. Dashed arrows indicate direction of temperature change. In the inset, the segment denotes range of Δf_a within which the determined T_{ca1} lies (see text for details).
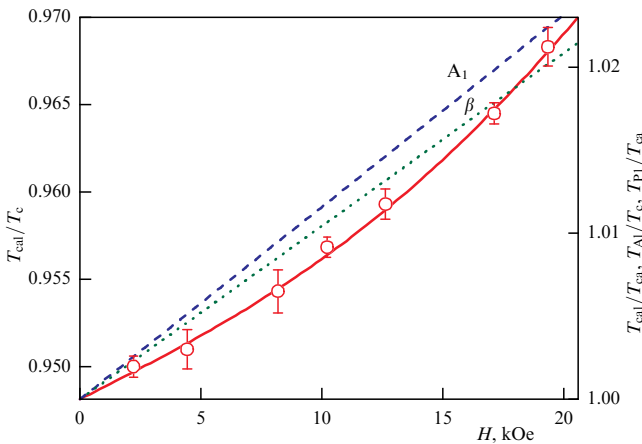
Figure 12. Temperature of 'upper' transition of ^{3}He in nematic aerogel to superfluid state in the absence of ^{4}He coating as a function of H (circles, left and right axes) [58]. Solid line is a fit of data to Eqn (10) using η_{A_1} and C_1 as fitting parameters. Right axis: temperatures of transition to A_1 phase in bulk ^{3}He (dashed line) and to β phase of ^{3}He in the same aerogel sample coated with ^{4}He [50] (dotted line).

detect specific field-dependent features that could be associated with transitions at $T = T_{ca2}$. Note that the peak change in Δf_a associated with the interaction with an additional resonance mode in pure ^{3}He occurs in a fairly wide temperature range and, presumably, the feature associated with the 'lower' transition is difficult to detect, since it is within this range.

Figure 12 shows the measured T_{ca1} versus H in pure ^{3}He. The same figure shows approximations of the experimental data for the temperatures of transitions to the A_1 phase (T_{A_1}/T_c) in bulk ^{3}He and to the β phase (T_{P_1}/T_{ca}) in ^{3}He filling the same aerogel sample but in the presence of a ^{4}He coating [50]. The solid line is the approximation of our data to Eqn (10) using η_{A_1} and C_1 as fitting parameters. Although the approximation looks reasonable, it contradicts our expectations. The fact is that the value of η_{A_1} obtained by fitting is 2.5 times larger than η_{A_1} in bulk ^{3}He. It is also seen that, if $H \gtrsim 15$ kOe, the dT_{ca1}/dH derivative exceeds the value of the

dT_{A_1}/dH derivative, whereas it should only reach this value, and only in magnetic fields of $H \gtrsim 70$ kOe ($h \gtrsim 2.5$).

To understand the observed deviation from the expected dependences, further theoretical studies are needed, as are experiments in stronger magnetic fields. One of the reasons for the discrepancies may be that the original theory [56, 57] was constructed for an isotropic aerogel, and, although the requirement of isotropy of quasiparticle scattering is not introduced anywhere in these studies, the theory for describing processes in nematic aerogel may turn out to be somewhat more complicated. Anyway, it is worth noting that the mentioned theories have not been finally tested either in an isotropic aerogel, in which experiments were carried out only in low magnetic fields, where the splitting of T_{ca} was not observed, or in fields of $H \gtrsim 70$ kOe, where the dependence of the splitting on H was already linear.

5. Conclusion

Using a vibrating wire with aerogel glued to it, we were able to observe superfluid transitions in ^{3}He in nematic aerogel into the polar, β, and distorted A and β phases, as well as into the A_1 phase. We found that, in nematic aerogel, the transition of ^{3}He into the superfluid phase is accompanied by the appearance of a second resonance mode inside the aerogel sample, which had not been observed previously in similar experiments with isotropic aerogel [31–34].

When studying the β phase, the splitting P_1–P_2 of the superfluid transition temperature of ^{3}He in nematic aerogel in strong magnetic fields was measured. It was found that the temperature range of the β phase existence is proportional to H.

In experiments with ^{3}He in nematic aerogel in the absence of a ^{4}He coating, the field dependence of the superfluid transition temperature of ^{3}He to the A_1 phase in aerogel was measured in magnetic fields up to 20 kOe. It was found that this dependence is nonlinear, and the growth of the transition temperature with increasing H is suppressed compared to the bulk A_1 phase. We associate this suppression with the influence of the magnetic scattering on the splitting of the superfluid transition temperature, as predicted in theoretical studies [56, 57]. However, a significant quantitative discrepancy with theoretical expectations is observed, for the explanation of which additional experimental and theoretical studies are needed.

References

1. Vollhardt D, Wölfle P *The Superfluid Phases of Helium 3* (London: Taylor and Francis, 1990)
2. Marchenko V I *Sov. Phys. JETP* **66** 79 (1987); *Zh. Eksp. Teor. Fiz.* **93** 141 (1987)
3. Mackenzie A P, Maeno Y *Rev. Mod. Phys.* **75** 657 (2003)
4. Dean D J, Hjorth-Jensen M *Rev. Mod. Phys.* **75** 607 (2003)
5. Ambegaokar V, Mermin N D *Phys. Rev. Lett.* **30** 81 (1973)
6. Israelsson U E et al. *Phys. Rev. Lett.* **53** 1943 (1984)
7. Sagan D C et al. *Phys. Rev. Lett.* **53** 1939 (1984)
8. Aoyama K, Ikeda R *Phys. Rev. B* **73** 060504 (2006)
9. Sauls J A *Phys. Rev. B* **88** 214503 (2013)
10. Fomin I A *J. Exp. Theor. Phys.* **118** 765 (2014); *Zh. Eksp. Teor. Fiz.* **145** 871 (2014)
11. Ikeda R *Phys. Rev. B* **91** 174515 (2015)

12. Fomin I A *J. Exp. Theor. Phys.* **127** 933 (2018); *Zh. Eksp. Teor. Fiz.* **154** 1034 (2018)
13. Volovik G E *JETP Lett.* **107** 324 (2018); *Pis'ma Zh. Eksp. Teor. Fiz.* **107** 340 (2018)
14. Fomin I A *J. Exp. Theor. Phys.* **131** 29 (2020); *Zh. Eksp. Teor. Fiz.* **158** 37 (2020)
15. Fomin I A *JETP Lett.* **114** 232 (2021); *Pis'ma Zh. Eksp. Teor. Fiz.* **114** 269 (2021)
16. Barker B I et al. *Phys. Rev. Lett.* **85** 2148 (2000)
17. Gervais G et al. *Phys. Rev. Lett.* **87** 035701 (2001)
18. Dmitriev V V et al. *JETP Lett.* **76** 312 (2002); *Pis'ma Zh. Eksp. Teor. Fiz.* **76** 371 (2002)
19. Dmitriev V V et al. *JETP Lett.* **91** 599 (2010); *Pis'ma Zh. Eksp. Teor. Fiz.* **91** 669 (2010)
20. Pollanen J et al. *Nature Phys.* **8** 317 (2012)
21. Li J I A et al. *Nature Phys.* **9** 775 (2013)
22. Li J I A et al. *Phys. Rev. Lett.* **112** 115303 (2014)
23. Li J I A et al. *Phys. Rev. Lett.* **114** 105302 (2015)
24. Dmitriev V V et al. *Phys. Rev. Lett.* **115** 165304 (2015)
25. Dmitriev V V, Soldatov A A, Yudin A N *J. Exp. Theor. Phys.* **131** 2 (2020); *Zh. Eksp. Teor. Fiz.* **158** 6 (2020)
26. Dmitriev V V et al. *J. Exp. Theor. Phys.* **119** 1088 (2014); *Zh. Eksp. Teor. Fiz.* **146** 1242 (2014)
27. Asadchikov V E et al. *JETP Lett.* **101** 556 (2015); *Pis'ma Zh. Eksp. Teor. Fiz.* **101** 613 (2015)
28. Askhadullin R Sh et al. *J. Phys. Conf. Ser.* **400** 012002 (2012)
29. Dmitriev V V et al. *JETP Lett.* **101** 808 (2015); *Pis'ma Zh. Eksp. Teor. Fiz.* **101** 908 (2015)
30. Dmitriev V V, Soldatov A A, Yudin A N *Phys. Rev. Lett.* **120** 075301 (2018)
31. Brussaard P et al. *J. Low Temp. Phys.* **121** 555 (2000)
32. Brussaard P et al. *Phys. Rev. Lett.* **86** 4580 (2001)
33. Bradley D I et al. *Phys. Rev. Lett.* **98** 075302 (2007)
34. Bradley D I et al. *J. Low Temp. Phys.* **150** 445 (2008)
35. Carless D C, Hall H E, Hook J R *J. Low Temp. Phys.* **50** 583 (1983)
36. Carless D C, Hall H E, Hook J R *J. Low Temp. Phys.* **50** 605 (1983)
37. Tough J T, McCormick W D, Dash J G *Rev. Sci. Instrum.* **35** 1345 (1964)
38. Gabay C, Wolf P E, Puech L *Physica B* **284–288** 97 (2000)
39. Blaauwgeers R et al. *J. Low Temp. Phys.* **146** 537 (2007)
40. Dmitriev V V et al. *JETP Lett.* **112** 780 (2020); *Pis'ma Zh. Eksp. Teor. Fiz.* **112** 820 (2020)
41. Dmitriev V V et al. *JETP Lett.* **110** 734 (2019); *Pis'ma Zh. Eksp. Teor. Fiz.* **110** 748 (2019)
42. McKenna M J, Slawecki T, Maynard J D *Phys. Rev. Lett.* **66** 1878 (1991)
43. Golov A et al. *Phys. Rev. Lett.* **82** 3492 (1999)
44. Nazaretski E, Lee D M, Parpia J M *Phys. Rev. B* **71** 144506 (2005)
45. Surovtsev E V *J. Exp. Theor. Phys.* **133** 477 (2021); *Zh. Eksp. Teor. Fiz.* **160** 553 (2021)
46. Surovtsev E V *JETP Lett.* **116** 745 (2022); *Pis'ma Zh. Eksp. Teor. Fiz.* **116** 724 (2022)
47. Surovtsev E V *JETP Lett.* **118** 759 (2023); *Pis'ma Zh. Eksp. Teor. Fiz.* **118** 754 (2023)
48. Surovtsev E V *J. Exp. Theor. Phys.* **128** 477 (2019); *Zh. Eksp. Teor. Fiz.* **155** 554 (2019)
49. Surovtsev E V *J. Exp. Theor. Phys.* **129** 1055 (2019); *Zh. Eksp. Teor. Fiz.* **156** 1158 (2019)
50. Dmitriev V V et al. *Phys. Rev. Lett.* **127** 265301 (2021)
51. Choi H C et al. *Phys. Rev. B* **75** 174503 (2007)
52. Dmitriev V V et al. *J. Low Temp. Phys.* **208** 3 (2022)
53. Gervais G et al. *Phys. Rev. B* **66** 054528 (2002)
54. Choi H C et al. *Phys. Rev. Lett.* **93** 145302 (2004)
55. Choi H C et al. *J. Low Temp. Phys.* **138** 107 (2005)
56. Sauls J A, Sharma P *Phys. Rev. B* **68** 224502 (2003)
57. Baramidze G A, Kharadze G A *J. Low Temp. Phys.* **135** 399 (2004)
58. Dmitriev V V et al. *Phys. Rev. B* **107** 024507 (2023)